Investigation of the extreme wet-cold compound events changes between 2025-2049 and 1980-2004 using regional simulations in Greece

Iason Markantonis[1,2], Diamando Vlachogiannis[1], Athanasios Sfetsos[1], Ioannis Kioutsioukis[2]

[1]Environmental Research Laboratory, NCSR "Demokritos", 15341 Agia Paraskevi, Greece

[2]University of Patras, Department of Physics, University Campus 26504 Rio, Patras, Greece

Correspondence to: Iason Markantonis (jasonm@ipta.demokritos.gr)

Abstract. This paper aims to study wet-cold compound events (WCCEs) in Greece for the wet and cold season November-April, since these events may affect directly human activities for short or longer periods as no similar research has been conducted for the country studying the past and future development of these compound events. WCCEs are divided in two different daily compound events (Maximum Temperature (TX) -Accumulated Precipitation (RR)) and (Minimum Temperature (TN) – Accumulated Precipitation (RR)) using fixed thresholds (RR over 20 mm/day and Temperature under 0 ^{o}C). Observational data from the Hellenic National Meteorology Service (HNMS) and simulation data from reanalysis and EURO-CORDEX models were used in the study for the historical period 1980-2004. The Ensemble mean of the simulation datasets from projection models were employed for the near future period (2025-2049) to study the impact of climate change on the occurrence of WCCEs under the Representative Concentration Pathways (RCPs) 4.5 and 8.5 scenarios. Following data processing and validation of the models, the potential changes in the distribution of WCCEs in the future were investigated based on the projected and historical simulations. WCCEs determined by fixed thresholds were mostly found over high altitudes with TN-RR events exhibiting a future tendency to reduce particularly under RCP 8.5 scenario and TX-RR exhibiting similar reduction of probabilities for both scenarios.

1. Introduction

Extreme weather events and their linkage to climate change is a matter of high concern for many scientific groups (Zanocco et al., 2018; Konisky et al., 2016; Curtis et al., 2017). In the last decade, numerous scientific studies focused on the causes, the frequency and impacts of extreme compound events (e.g. Aghakouchak et al., 2020; Singh et al., 2021; Sadegh et al., 2018; Zscheischler et al., 2017; Zscheischler and Seneviratne, 2017; Zscheischler et al., 2018). As mentioned in the Intergovernmental Panel on Climate Change report on "Managing the risks of extreme events and disasters to advance climate change adaptation" (IPCC SREX) (Ref 7, p. 118) compound events are defined as: (1) two or more extreme events occurring simultaneously or successively, (2) combinations of extreme events with underlying conditions that amplify the impact of the events, or (3) combination of events that are not themselves extremes but lead to an extreme event or impact when combined (Leonard et al., 2014).

Recent studies have been conducted on the examination of wet-cold compound events (WCCEs) that concern monthly extreme values of temperature and precipitation and the correlation of these variables (Lemus-Canovas, 2022; Chukwudum and Nadarajah, 2022; Lhotka and Kyselý, 2021; Wu et al., 2019). The purpose of this article is the study of extreme WCCEs on daily basis in Greece during the historical period (1980-2004) and howthe occurrence of these events will be affected by climate change. It has been reported that WCCEs affect the region of the Mediterranean Sea, including Greece (Zhang et al., 2021). Studies using only observational data at some locations (Lazoglou and Anagnostopoulou, 2019), or modeled data mostly over the broader region of the Mediterranean Sea (Vogel et al., 2021; Hochman et al., 2021; de Luca et al., 2020), concerning WCCEs have been conducted in the past, but not depicting analytically WCCEs in Greece, which is attempted in this work.

The examined events belong to the first category of the definition of compound events from IPCC since they refer to the simultaneous exceedance of precipitation and temperature thresholds. WCCEs may have a negative impact on people's lives by causing electricity blackouts, affecting agriculture

with heavy snowfall or freezing rain andblocking transportation because of closed roads, railways or even airports (Houston et al., 2006; Llasat et al., 2014; Vajda et al., 2014). On the other hand, most of the available freshwater in the country comes from melted mountain snow during spring or summer. Finally, eco-systems, especially in mountains, may be affected by the absence of snow that climate change may cause (Demiroglu et al., 2015; Pestereva et al., 2012; Trujillo et al., 2012; García-Ruiz et al., 2011).

The first part of the study concerns the historical period between 1980 and 2004, because of the availability of quality controlled daily observational data for minimum temperature (TN), maximum temperature (TX) and accumulated precipitation (RR). Hence, for that period, we use observational data from 21 Hellenic National Meteorological Service (HNMS) stations, to validate EURO-CORDEX Regional Climate Models (RCMs), provided by the Copernicus Climate Change Service and the projection model dataset produced in-house. In addition to the models, two reanalysis products are included, as the closest to "true" past climate conditions in regions with no or scarce observations (Moalafhi et al., 2016). More information about the observational and model datasets is presented in Section 2. Section 3 highlights the applied methodology while Section 4 displays WCCEs observed in stations and station cells of the models and Section 5 contains reanalysis and projections Ensemble mean WCCEs probabilities spatial distribution for the historical period. Section 6 details the results about the difference in WCCEs probabilities between the historical and the near future period between 2025 and 2049 for two greenhouse gas concentration scenarios, RCP 4.5 and RCP 8.5.

2. Data

In this Section, we present the datasets that provide the observational and simulation data produced by projection and reanalysis models.

1. HNMS observations

HNMS provides freely observational data from 21 stations for the purpose of scientific research (http://www.emy.gr/emy/el/services/paroxi-ipiresion-elefthera-dedomena). The data have been formally evaluated by HNMS and the timeseries show no missing or distorted values. In particular, the timeseries available for the historical period 1980-2004 have a 3-hour temporal resolution and from these values we have extracted the daily values of TN, TX and RR. Figure 1 shows the position of the stations while Table A1 of Appendix A provides details on the characteristics of the stations. We have used the observational data to validate the model datasets regarding the WCCEs for the historical period.

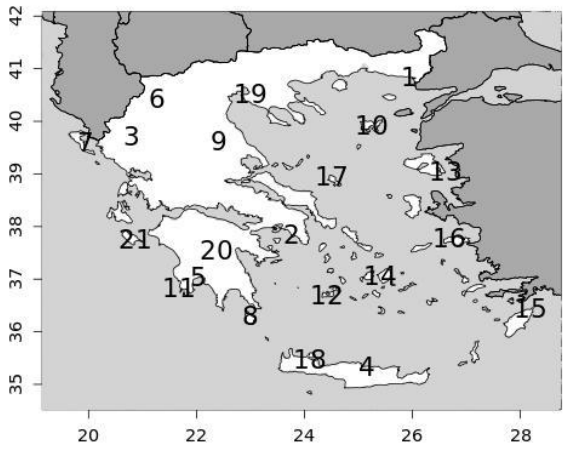

Figure 1: Map of HNMS stations. The numbers correspond to those in Table A1 (Appendix A).

2.2 Reanalysis models

We have used two reanalysis models due to the lack of spatially and temporally complete direct observations, to study more consistently the WCCEs in Greece in the historical period. The first model is the latest available reanalysis product ERA 5 from the European Centre for Medium-Range Weather Forecasts (ECMWF) of spatial resolution ~30km x 30km (Hersbach et al., 2020). The second reanalysis model, built in the Environmental Research Laboratory (EREL) of National Center of Scientific Research 'Demokritos' (NCSRD) WRF_ERA_I, has been produced by dynamically downscaling ERA-INTERIM using the Weather Research Forecast (WRF) model (v3.6.1) from 80km x 80km to 5km x 5km (Politi et al., 2021, 2020, 2018).

2.3 GCM / RCM models

To observe possible alterations of WCCEs occurrence probability in the future period 2025-2049 compared to the historical period, we employed data from RCM simulations driven by GCMs. In this regard, we obtained data from 5 models included in the EURO-CORDEX initiative provided by the Copernicus Program. All chosen EURO-CORDEX models with available daily data for both RCP scenarios were selected because they have the finest spatial resolution of 0.11º x 0.11º, and have also been tested in Cardoso et al, (2019) (Cardoso et al., 2019). Information on the regional and parent models and their acronyms used herewith is given in Table 1. In addition to the EURO-CORDEX model data, we have used dynamically downscaled data from the EC-EARTH GCM to high spatial resolution of 5km x 5km for the area of Greece using the WRF model (Politi et al., 2020, 2022).

Institution	Reference	Regional Model	Forcing model	Acronym	Resolution (°)
Météo-France / Centre National de Recherches Météorologiques	(Spiridonov et al., n.d.)	ALADIN63	CNRM-CERFACS-CNRM-CM5	CNRM	0.11
Koninklijk Nederlands Meteorologisch Instituut	(van Meijgaard et al., 2008)	KNMI-RACMO22E	ICHEC-EC-EARTH	KNMI	0.11
Climate Limited-Area Modelling Community	(Rockel et al., 2008)	CLMcom-CLM-CCLM4-8-17	MOHC-HadGEM2-ES	CLMcom	0.11
Swedish Meteorological and Hydrological Institute	(Samuelsson et al., 2016)	SMHI-RCA4	MPI-M-MPI-ESM-LR	SMHI	0.11
Danish Meteorological Institute	(Christensen, 2006)	DMI-HIRHAM5	NCC-NorESM1-M	DMI	0.11
EREL (NCSRD)	(Politi et al. 2020, 2022)	ARW-WRF	EC-EARTH	WRF_EC	0.05

Table 1: EURO-CORDEX and EREL-NCSRD simulation models information.

3. Methodology

The first step in this study is the validation of the projection and reanalysis models against observations. Moreover, the ensemble of the 6 projection models is also exhibited. We choose as the Ensemble resolution that of the CORDEX models since 5 of them share the same spatial resolution. The only model in need of regridding is WRF_EC. We follow the nearest neighbor method to upscale WRF_EC from 5 km to 11 km. In addition, we use box-plots to depict the ability of the models to simulate observational data WCCEs probabilities for the historical period at the cells that include

meteorological stations. The box-plots consist of the colored box, where in the band near the middle of the box is the median, the bottom and top of each color box are the 25th (Q1) and 75th (Q3) percentiles (BL) percentile The lower limit of the whisker (LLW) is calculated by LW= Q1-1.5*BL and the upper limit (ULW) by UW= Q3+1.5*BL. The length of the whiskers (WL) is calculated as the difference between ULW and LLW. Any value out of this range is marked by a black point in the plot. The validation is conducted after the elevation bias correction of temperature at the cells of the models containing the stations. The cells of the stations are found using the nearest neighbor approach and the temperature bias correction temperature is the following:

$$T_s = T_m + 0.06*(H_m-H_s) \quad (1)$$

In equation (1), T_s is the temperature of the cell after the elevation bias correction, T_m the temperature provided by the model, H_m the cell elevation and H_s the elevation of the HNMS station.

3.1 Compound event selection

According to HNMS, the meteorological year can be split into two climate periods (http://emy.gr/emy/el/climatology/climatology). The cold and wet period extends on average from mid-October to the end of March, and the warm-dry period occurs during the rest of the year. Since the study is focused on the extreme WCCEs, we examine the period between November and April, since according to the HNMS observations, April exhibits lower temperatures than October and more rainy days. Moreover, it is not uncommon for the northern parts of Greece, and especially mountainous areas, to be affected by snowfalls during April. This leads to the creation of a timeseries of 4532 daily values for the historical period and 4531 for the future period. CLMcom considers that each month is consisted by 30 days, thus leading to 4500 values for each period. Also, DMI considers that a calendar year has 365 days, thus each period examined has 4525 values.

The WCCEs, which are examined on daily basis, are divided in two types of synchronous events, TX-RR and TN-RR and studied using the fixed threshold approach (Table 2). This approach considers the fixed threshold of 20 mm/day for RR and 0 °C for TN and TX for all stations or grid points, as recommended by the Commission for Climatology (CCl), the World Climate Research Programme (WCRP) of the Climate Variability and Predictability Component (CLIVAR) project and the Expert Team for Climate Change Detection and Indices (ETCCDI). TN equal to or under 0 °C indicates Frost Days (FD), while TX equal or under 0 °C Iced Days (ID) (Fonseca et al., 2016). The thresholds examined have been proposed in various works for studying extreme events (Raziei et al., 2014; Tošić and Unkašević, 2013; Anagnostopoulou and Tolika, 2012; Pongrácz et al., 2009; Kundzewicz et al., 2006; Moberg et al., 2006)..

THRESHOLDS	RR	TN	TX	WCCE
FIXED	>= 20 mm/day **(RR20)**	<= 0 ºC **(FD)**	<= 0 ºC **(ID)**	**1. (RR20-FD)** **2. (RR20-ID)**

Table 2: Univariate thresholds and the compound events examined in the study.

3.2 WCCEs probability calculation

The WCCEs probabilities are calculated by applying two different methods. The first is the empirical approach counting the events from the timeseries and dividing by the total number of days to find the percentage (%) of the occurrence probability. For the second method, we use the copula approach for the HNMS observations and model comparison and to map the differences between the two methods for the reanalysis and projection of model data. Compared to copula, an empirical method has a higher uncertainty when calculating the probability of extreme events (Hao et al., 2018; Tavakol et al., 2020; Zscheischler and Seneviratne, 2017). The purpose of using two different methods is to investigate whether the copula method underestimates or overestimates the WCCEs.

The best fitting copula selection for each timeseries is examined using the R programming language function BiCopSelect as suggested in (Zhou et al., 2019) package VineCopula (Schepsmeier et al., 2013). The appropriate bivariate copula for each dataset is chosen by the function, from a multitude of 40 different copula families using the Akaike Information Criterion (AIC) (Akaike, 1974) and Bayesian Information Criterion (BIC) (Schwarz, 1978), and the copula chosen for each station and model dataset is shown in Appendix B (Tables B1 and B2). Copulas are used in plenty of studies that investigate the dependence between two different climate variables and the joint probability of compound events (Tavakol et al., 2020; Dzupire et al., 2020; Pandey et al., 2018; Cong and Brady, 2012; Abraj and Hewaarachchi, 2021).

As mentioned in Nelsen, (2007), a bivariate copula is a bivariate distribution function where margins are uniform on the unit interval [0, 1]. A bivariate copula is a map $C:[0,1]^2 \rightarrow [0,1]$ with $C(u,1)=u$ and $C(1,v)=v$. Let X and Y be random variables with a joint distribution function $F(x,y)=Pr(X \leq x, Y \leq y)$ and continuous marginal distribution functions $F_1(x)=Pr(X \leq x)$ and $F_2(y)=Pr(Y \leq y)$, respectively. By Sklar's theorem (Sklar, 1959), one obtains a unique representation

$$F(x,y) = C\{F_1(x),F_2(y)\} \quad (2)$$

For the two random variables of X (e.g., precipitation) and Y (e.g., temperature) with cumulative distribution functions (CDFs) $F_1(x)=Pr(X>=x)$ and $F_2(y)=Pr(Y<=y)$, the bivariate joint distribution function or copula (C) can be written as:

$$F(x,y) = Pr(X>=x,Y<=y) = C(u,v) \quad (3)$$

4. WCCEs assessment in HNMS stations

In this section, the models are validated against observations both for the empirical and the copula method. WCCEs probabilities for each station and model are presented in the supplementary material. BIAS and RMSE along with the Critical Success Index (CSI) are used for the validation. CSI is calculated as: CSI=A/(A+B+C). A, B and C symbolize elements from the contingency table (Table 2) that occur from comparing zero and non-zero probabilities in stations with the corresponding model cells. Also, total number of events calculated for both methods from observational data are presented in each station.

"EVENT"=POSITIVE PROBABILITY		OBSERVATION EVENT	
		YES	NO
MODEL EVENT	YES	**A**	**B**
	NO	**C**	**D**

Table 2: Contingency table where "A" is the number of event forecasts that correspond to event observations, or the number of hits. Entry "B" is the number of event forecasts that do not correspond to observed events, or the number of false alarms. Entry "C" is the number of no-event forecasts corresponding to observed events, or the number of misses. Entry "D" is the number of no-event forecasts corresponding to no events observed, or the number of correct rejections.

4.1 RR20FD

Probability values for each station are presented in Supplementary (Tables S1-S4) as well as the contingency tables (Tables S7-S10) from which CSI is calculated. ERA5 and WRF_ERA_I are reanalysis products and exhibited for comparison reasons. The copulas selected by Bicopselect for each observational and modeled timeseries are also presented in Supplementary (Tables S5-S6).

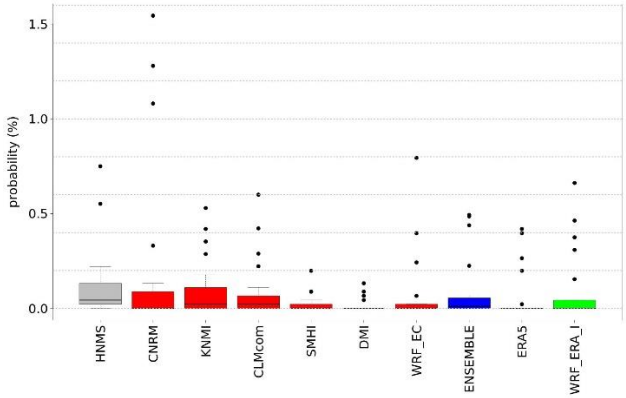

Figure 2: Box-plot presenting RR20FD empirical method probabilities for observations and models.

	HNMS	*CNRM*	*KNMI*	*CLMcom*	*SMHI*	*DMI*	*WRF_EC*	*ENSEMBLE*	*ERA5*	*WRF_ERA_I*
MEAN	**0.1177**	0.2217	0.0977	0.0899	0.0252	0.0158	0.0935	**0.0906**	0.0620	0.0988
SD	**0.1912**	0.4641	0.1600	0.1622	0.0480	0.0364	0.2034	**0.1674**	0.1347	0.1886
BIAS		-0.1040	0.0199	0.0277	0.0924	0.1019	0.0242	**0.0270**	0.0557	0.0189
RMSE		0.3410	0.1216	0.0929	0.1718	0.2029	0.1131	**0.0989**	0.1273	0.1117
COR		0.7958	0.7689	0.8804	0.9183	0.4000	0.8371	**0.8604**	0.7949	0.8235
CSI		0.4762	0.5500	0.5000	0.4000	0.1905	0.3500	**0.6842**	0.2381	0.4000

Table 3: Table exhibiting mean (MEAN) station RR20FD empirical probabilities probabilities (%) for observations and models, standard deviation (SD), bias (BIAS), rmse (RMSE), Pearson correlation (COR) and CSI of models against observations.

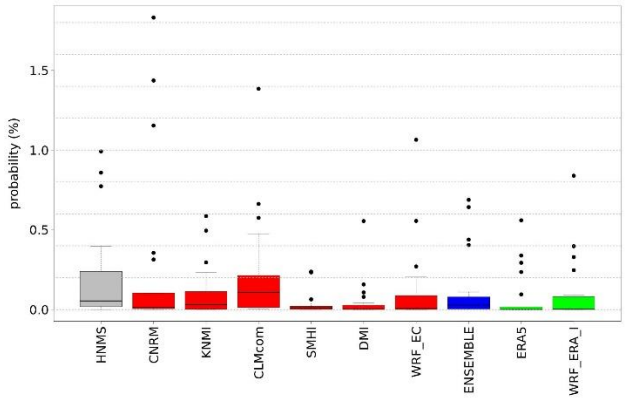

Figure 3: Box-plot presenting RR20FD copula method probabilities for observations and models.

	HNMS	*CNRM*	*KNMI*	*CLMcom*	*SMHI*	*DMI*	*WRF_EC*	*ENSEMBLE*	*ERA5*	*WRF_ERA_I*
MEAN	**0.2032**	0.2592	0.1030	0.2096	0.0341	0.0495	0.1130	**0.1281**	0.0742	0.0995
SD	**0.3014**	0.5283	0.1686	0.3323	0.0689	0.1232	0.2558	**0.2160**	0.1524	0.2053
BIAS		-0.0560	0.1002	-0.0064	0.1691	0.1537	0.0902	**0.0751**	0.1290	0.1037
RMSE		0.2493	0.1891	0.2672	0.2962	0.2743	0.1573	**0.1320**	0.2129	0.1690
COR		0.9671	0.9079	0.6307	0.8053	0.6979	0.9004	**0.9610**	0.9140	0.9236
CSI		0.8889	0.9444	1.0000	0.9474	0.6190	0.7500	**1.0000**	0.5238	0.7000

Table 4: Table exhibiting mean (MEAN) RR20FD copula probabilities station probabilities (%) for observations and models, standard deviation (SD), bias (BIAS), rmse (RMSE), Pearson correlation (COR) and CSI of models against observations.

Figure 4 shows that (RR20-FD) events display higher numbers, mostly in the mainland. At several stations, there is a difference between the empirical and the copula approach, which in stations overestimates the total number of WCCEs.

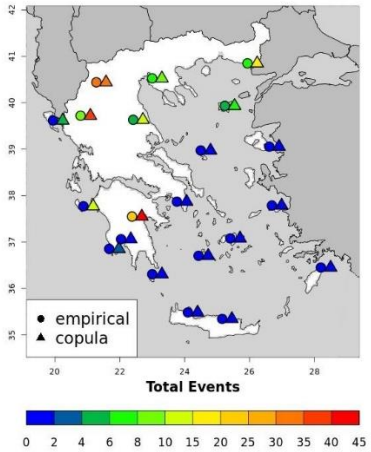

Figure 4: Total number of RR20FD WCCEs (1980-2004). Circles symbolize empirical and triangles the copula method.

4.2 RR20ID

RR20ID events yield, as expected, lower probabilities than RR20FD events as observed in Figures 5 and 6. Most observations and models yield zero probabilities, hence validation of models for these events is limited. The empirical method exhibits only two stations with events in the historical period (Figure 7).

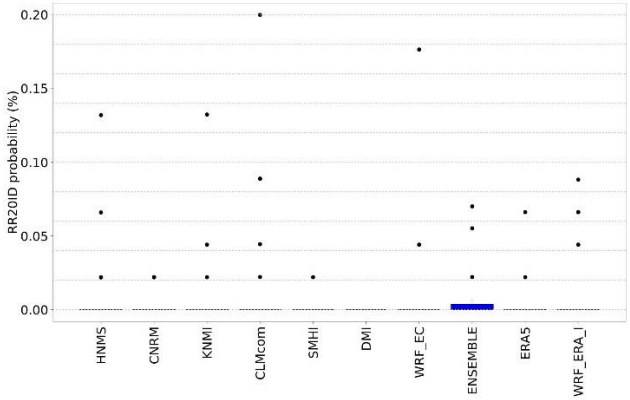

Figure 5: Box-plot presenting RR20ID empirical method probabilities for observations and models.

	HNMS	*CNRM*	*KNMI*	*CLMcom*	*SMHI*	*DMI*	*WRF_EC*	*ENSEMBLE*	*ERA5*	*WRF_ERA_I*
MEAN	**0.0115**	0.0032	0.0095	0.0212	0.0011	0.0000	0.0126	**0.0079**	0.0042	0.0147
SD	**0.0316**	0.0079	0.0301	0.0494	0.0048	0.0000	0.0398	**0.0191**	0.0150	0.0282
BIAS		0.0084	0.0021	-0.0096	0.0105	0.0115	-0.0011	**0.0036**	0.0073	-0.0032

RMSE		0.0263	0.0068	0.0280	0.0288	0.0329	0.0330	**0.0157**	0.0220	0.0231
COR		0.8185	0.9782	0.8692	0.8738	NA	0.5733	**0.9256**	0.8149	0.6993
CSI		0.1429	0.1429	0.1111	0.0476	0.0000	0.1000	**0.1667**	0.0500	0.1579

Table 5: Table exhibiting mean (MEAN) RR20ID emprirical probabilities station probabilities (%) for observations and models, standard deviation (SD), bias (BIAS), rmse (RMSE), Pearson correlation (COR) and CSI of models against observations.

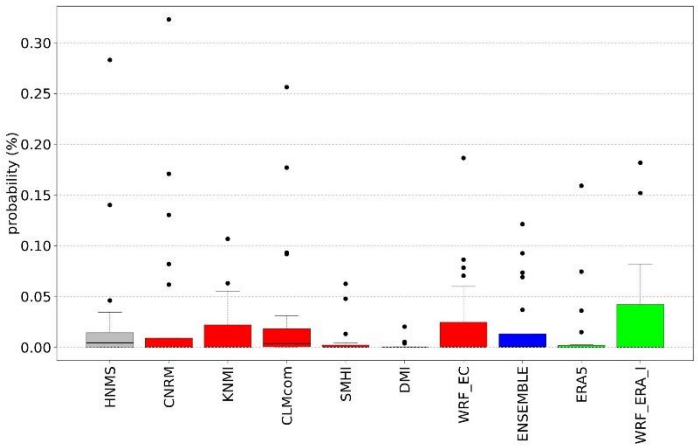

Figure 6: Box-plot presenting RR20ID copula method probabilities for observations and models.

	HNMS	***CNRM***	***KNMI***	***CLMcom***	***SMHI***	***DMI***	***WRF_EC***	***ENSEMBLE***	***ERA5***	***WRF_ERA_I***
MEAN	**0.0282**	0.0378	0.0169	0.0344	0.0066	0.0017	0.0249	**2.040E-02**	0.0138	0.0274
SD	**0.0663**	0.0811	0.0303	0.0676	0.0166	0.0046	0.0473	**3.640E-02**	0.0377	0.0524
BIAS		-0.0097	0.0112	-0.0062	0.0215	0.0264	0.0032	**0.0078**	0.0144	0.0008
RMSE		0.0532	0.0493	0.0598	0.0565	0.0691	0.0489	**0.0443**	0.0420	0.0339
COR		0.7534	0.7228	0.5861	0.8202	0.2291	0.6594	**0.7712**	0.8370	0.8540
CSI		0.4000	0.3810	0.7857	0.4737	0.3333	0.4211	0.7857	0.2857	0.35

Table 6: Table exhibiting mean (MEAN) RR20ID copula probabilities station probabilities (%) for observations and models, standard deviation (SD), bias (BIAS), rmse (RMSE), Pearson correlation (COR) and CSI of models against observations.

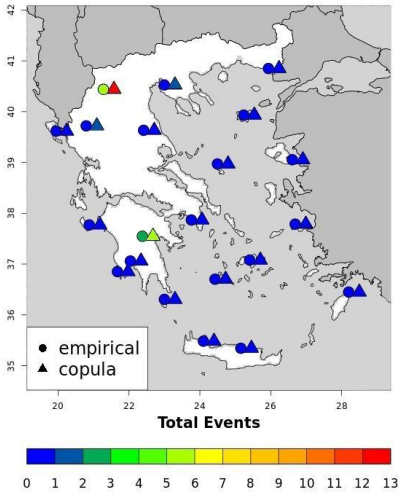

Figure 7: Total number of RR20ID WCCEs (1980-2004). Circles symbolize empirical and triangles the copula method.

4.3 Observations-models comparison conclusions

The events examined are rare among the available stations for the historical period. Copulas considering the dependence between the variables yield greater probabilities than the empirical method. More stations with non-zero probabilities enable more accurate validation of the models. To minimize uncertainties, smooth extreme underestimations or overestimations of WCCE probabilities that each model yields, and because ENSEMBLE shows better consistency among the projection models' statistical indices, we use it for further analysis in the study.

5. Historical period models WCCEs on maps

In this section, WCCEs spatial distribution probabilities are compared between empirical and copula methods. This procedure is conducted separately for the two reanalysis products and the Ensemble mean of the projection models.

5.1 Reanalysis

ERA5 and WRF_ERA_I WCCEs spatial distribution probabilities in Greece are displayed in this section. We display both reanalysis products, although ERA5 is the most recently developed reanalysis product, we exhibit also WRF_ERA_I since its much finer spatial resolution is more appropriate for the complex topography of Greece with many mountains and islands.

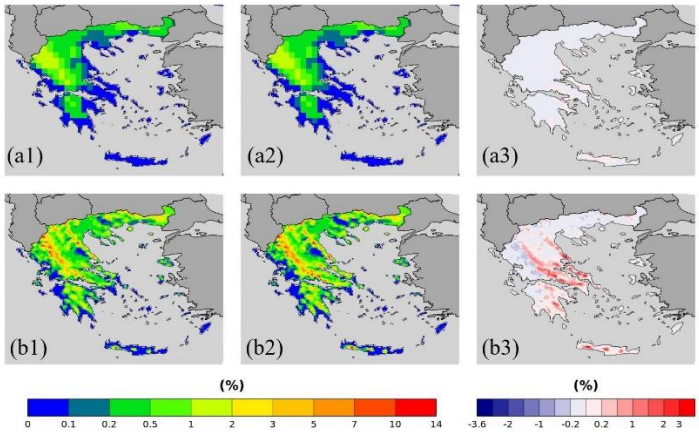

Figure 8: RR20FD probabilities for (a) ERA5 and (b) WRF_ERA_I produced by (1) Empirical and (2) Copula and (3) = (2) –(1).

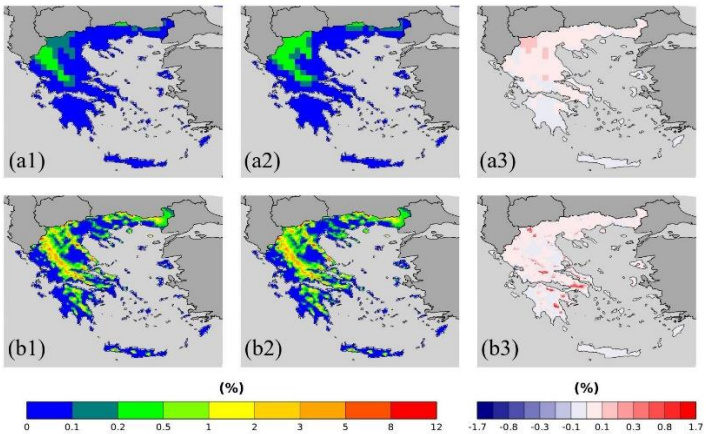

Figure 9: RR20ID probabilities for (a) ERA5 and (b) WRF_ERA_I produced by (1) Empirical and (2) Copula and (3) = (2) –(1).

Both reanalysis products yield greater WCCEs probabilities in the Pindus mountains, although due to its finer spatial resolution, WRF_ERA_I display high probabilities at other mountainous regions located in Crete, Peloponnese, Evia Island and others. Also, in both WCCEs copula method yields higher probabilities, especially for WRF_ERA_I and the RR20FD case. Moreover, WRF_ERA_I displays a greater range than ERA5 with RR20FD probabilities reaching 14% and RR20ID 12% compared to 6% and 2% of ERA5 respectively.

5.2 Projections Ensemble

Figures 10 and 11 yield that the Ensemble mean displays similar to WRF_ERA_I spatial distribution of WCCEs. RR20FD and RR20ID probabilities reach 10.8% and 5.4% respectively. The copula method yields higher probabilities for both methods in mountainous regions with greater difference displayed for RR20ID events in the Pindus mountain range and RR20FD exhibiting greater spatial distribution in differences between the two methods.

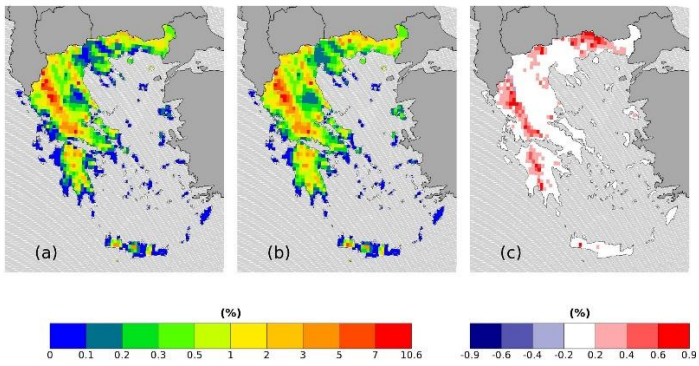

Figure 10: RR20FD Ensemble probabilities for (a) Empirical and (b) Copula method. (c)=(b)-(a).

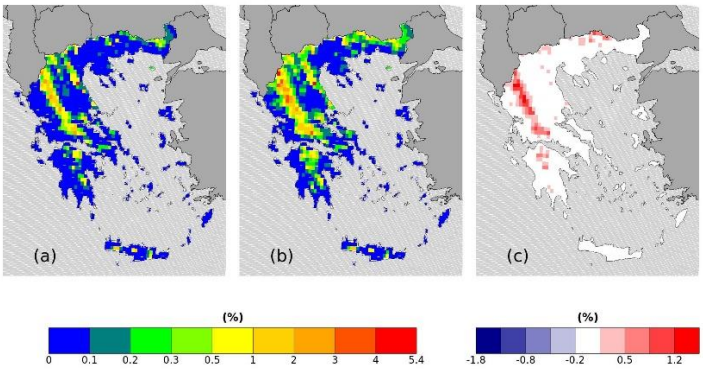

Figure 11: RR20ID Ensemble probabilities for (a) Empirical and (b) Copula method. (c)=(b)-(a).

6. Past-Future Ensemble differences

This section displays the differences of the Ensemble mean WCCEs probabilities, calculated for the empirical and the copula method, compared to the past probabilities presented in the previous section. The differences mapped are statistically significant at a 95% level using the Student's t-test (Goulden, 1939) comparing 25 annual values of the timeseries.

6.1 RR20FD

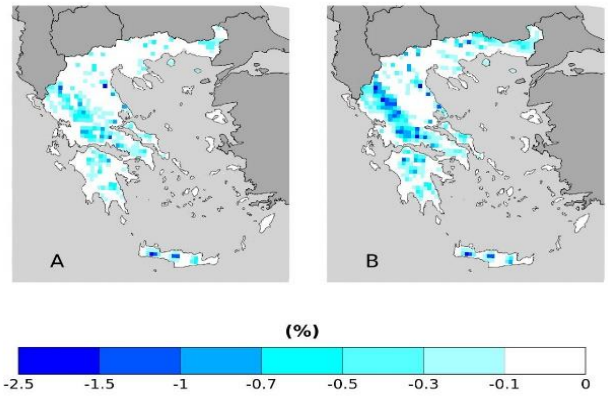

Figure 12: RR20FD empirical method probability differences of future-past periods for (A) RCP4.5 and (B) RCP8.5 scenarios.

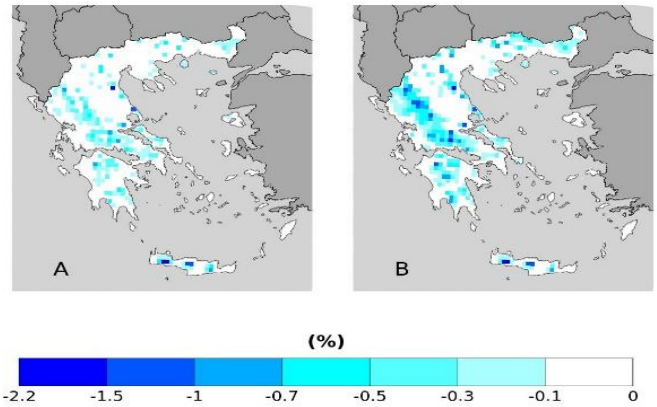

Figure 13: RR20FD copula method probability differences of future-past periods for (A) RCP4.5 and (B) RCP8.5 scenarios.

	Empirical RCP4.5	*Empirical RCP8.5*	*Copula RCP4.5*	*Copula RCP8.5*
0<=Nc>-0.1	**34**	**31**	**64**	**57**
-0.1<=Nc>-0.3	**112**	**154**	**112**	**131**
-0.3<=Nc>-0.5	**63**	**65**	**53**	**81**
-0.5<=Nc>-0.7	**31**	**48**	**16**	**47**
-0.7<=Nc>-1	**12**	**34**	**6**	**24**
-1<=Nc>-1.5	**5**	**18**	**3**	**11**
Nc<=-1.5	**2**	**5**	**3**	**4**
MAX D	**-1.8063 %**	**-2.4988 %**	**-1.9500 %**	**-2.1392 %**

Table 7: ENSEMBLE Number of cells (Nc) in each category of probability difference (%) for RR20FD for empirical and copula method. MAX D denotes the maximum negative difference between future and past periods. Nv concerns only cells with statistically significant difference.

From the results displayed in Figures 12 and 13 and in Table 7 RCP4.5 and RCP8.5 scenarios for the probabilities of the RR20FD events we observe that in all cases future scenarios yield only negative values, meaning the reduction of RR20FD events in 2025-2049 period compared to 1980-2004 period in all mountainous regions of Greece. RCP8.5 yields greater reduction of RR20FD probabilities than the RCP4.5 scenario both in spatial distribution and extreme values. The empirical method exhibits a greater reduction for the RCP8.5 scenario, although for the RCP4.5 scenario both methods yield similar results.

6.2 RR20ID

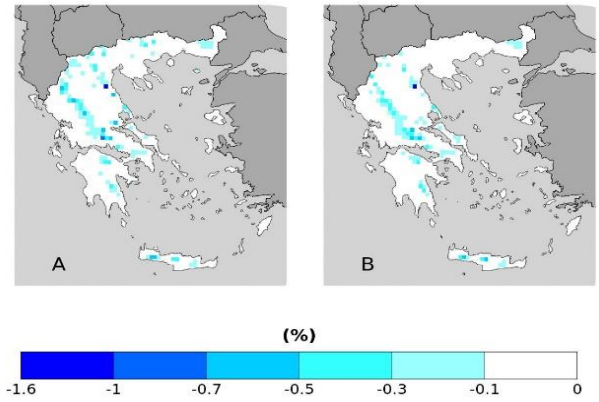

Figure 14: RR20ID empirical method probability differences of future-past periods for (A) RCP4.5 and (B) RCP8.5 scenarios.

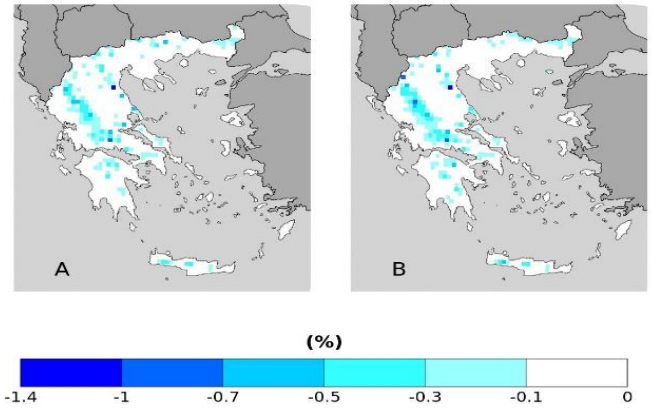

Figure 15: RR20ID copula method probability differences of future-past periods for (A) RCP4.5 and (B) RCP8.5 scenarios.

	Empirical RCP4.5	*Empirical RCP8.5*	*Copula RCP4.5*	*Copula RCP8.5*
0<=Nc>-0.1	193	229	166	210
-0.1<=Nc>-0.3	81	71	96	109
-0.3<=Nc>-0.5	23	20	33	37
-0.5<=Nc>-0.7	9	5	9	7
-0.7<=Nc>-1	1	0	1	3
Nc<=-1	1	1	1	1
MAX D	-1.5536	-1.0593	-1.3425	-1.1362

Table 8: ENSEMBLE Number of cells (Nc) in each category of probability difference (%) for RR20ID for empirical and copula method. MAX D denotes the maximum negative difference between future and past periods. Nv concerns only cells with statistically significant difference.

Similarly to RR20FD, RR20ID events probabilities yield only zero or negative differences compared to the past for both scenarios. Empirical and copula methods yield similar results in distribution and extreme values. For both methods, the RCP4.5 scenario tends to higher reduction of RR20ID probabilities than RCP8.5, as observed in Table 8.

Conclusions

This work presents for the first time to our knowledge an extensive study of wet-cold compound events in Greece for the historical and future periods of 1980-2004 and 2025-2049, respectively. Models' data from the EUROCORDEX initiative of 0.11° resolution and reanalysis data (ERA5 and ERA-Interim dynamically downscaled to 5km^2) were used and validated for the determined WCCEs against the formally available observational datasets by HNMS for the country. The number of events and their probabilities of occurrence were determined by applyinga fixed thresholds approach. Then, the bivariate validation of the models' datasets against observations was performed for the determined bivariate thresholds. The probabilities of WCCEs were computed using the empirical method and the best-fitted copula for the bivariate timeseries for observational data, reanalysis, projection models and the Ensemble of the projection models. Copulas yield higher extreme events probabilities for most of the cases considering the dependence between temperature and precipitation

Although, there is an absence of stations over mountainous areas we trust the results produced by models since bivariate validation shows good agreement between observations and models. This trust is enhanced by the fact that winter period systems affect large areas crossing the country from north to south or from west to east (Cartalis et al., 2010) and therefore recorded by available stations. Also, in the cold period of the year, convective precipitation forced by orography is limited hence the doubt that the models do not simulate extreme rainfall in winter is reduced. Moreover, the use of the Ensemble mean of the models reduces the probability of models' overestimation or underestimation of extreme events occurrences. The reduction of RR20-FD and RR20-ID WCCEs on mountains that the Ensemble of projection models predict in the future, might contribute to less heavy snowfall events and possibly less accumulated snow depth. If such a scenario will be verified, Greece faces the threat of losing the main sources of fresh water that come from melted mountain snow during spring or early summer in the near future. The rise of temperature due to global warming is the main factor for the reduction of WCCEs (Supplementary Figures S5-S7), thus similar mountainous regions in other parts of the planet face similar danger considering the unique characteristics of each area.

Acknowledgments

The authors acknowledge partial funding by the project "National Research Network for Climate Change and its Impacts, (CLIMPACT - 105658/17-10-2019)" of the Ministry of Development, GSRT, Program of Public Investment, 2019.

References

Abdi, H.: The Kendall Rank Correlation Coefficient, 2007.

Abraj, M. A. M. and Hewaarachchi, A. P.: Joint return period estimation of daily maximum and minimum temperatures using copula method, 66, 175–190, https://doi.org/10.17654/AS066020175, 2021.

Aghakouchak, A., Chiang, F., Huning, L. S., Love, C. A., Mallakpour, I., Mazdiyasni, O., Moftakhari, H., Papalexiou, S. M., Ragno, E., and Sadegh, M.: Climate Extremes and Compound Hazards in a Warming World, 48, 519–548, https://doi.org/10.1146/ANNUREV-EARTH-071719-055228, 2020.

Akaike, H.: A New Look at the Statistical Model Identification, 19, 716–723, https://doi.org/10.1109/TAC.1974.1100705, 1974.

Anagnostopoulou, C. and Tolika, K.: Extreme precipitation in Europe: Statistical threshold selection based on climatological criteria, 107, 479–489, https://doi.org/10.1007/S00704-011-0487-8/TABLES/2, 2012.

Balkema, A. A. and Haan, L. de: Residual Life Time at Great Age, 2, 792–804, https://doi.org/10.1214/AOP/1176996548, 1974.

Cartalis, C., Chrysoulakis, N., Feidas, H., and Pitsitakis, N.: International Journal of Remote Sensing Categorization of cold period weather types in Greece on the basis of the photointerpretation of NOAA/AVHRR imagery Categorization of cold period weather types in Greece on the basis of the

photointerpretation of NOAA/AVHRR imagery, https://doi.org/10.1080/01431160310001632684, 2010.

Cardoso, R. M., Soares, P. M. M., Lima, D. C. A., and Miranda, P. M. A.: Mean and extreme temperatures in a warming climate: EURO CORDEX and WRF regional climate high-resolution projections for Portugal, 52, 129–157, https://doi.org/10.1007/S00382-018-4124-4/FIGURES/8, 2019.

Christensen, O. B.: Regional climate change in Denmark according to a global 2-degree-warming scenario, 2006.

Chukwudum, Q. C. and Nadarajah, S.: Bivariate Extreme Value Analysis of Rainfall and Temperature in Nigeria, Environmental Modeling and Assessment, 27, 343–362, https://doi.org/10.1007/S10666-021-09781-7/TABLES/13, 2022.

Coles, S.: An Introduction to Statistical Modeling of Extreme Values, https://doi.org/10.1007/978-1-4471-3675-0, 2001.

Cong, R. G. and Brady, M.: The interdependence between rainfall and temperature: Copula analyses, 2012, https://doi.org/10.1100/2012/405675, 2012.

Curtis, S., Fair, A., Wistow, J., Val, D. v., and Oven, K.: Impact of extreme weather events and climate change for health and social care systems, 16, 23–32, https://doi.org/10.1186/S12940-017-0324-3/METRICS, 2017.

de Luca, P., Messori, G., Faranda, D., Ward, P. J., and Coumou, D.: Compound warm-dry and cold-wet events over the Mediterranean, 11, 793–805, https://doi.org/10.5194/ESD-11-793-2020, 2020.

Demiroglu, O. C., Kučerová, J., and Ozcelebi, O.: Snow reliability and climate elasticity: Case of a Slovak ski resort, 70, 1–12, https://doi.org/10.1108/TR-01-2014-0003/FULL/PDF, 2015.

Dzupire, N. C., Ngare, P., and Odongo, L.: A copula based bi-variate model for temperature and rainfall processes, 8, e00365, https://doi.org/10.1016/J.SCIAF.2020.E00365, 2020.

Fisher, R. A. and Tippett, L. H. C.: Limiting forms of the frequency distribution of the largest or smallest member of a sample, 24, 180–190, https://doi.org/10.1017/S0305004100015681, 1928.

Fonseca, D., Carvalho, M. J., Marta-Almeida, M., Melo-Gonçalves, P., and Rocha, A.: Recent trends of extreme temperature indices for the Iberian Peninsula, 94, 66–76, https://doi.org/10.1016/J.PCE.2015.12.005, 2016.

García-Ruiz, J. M., López-Moreno, I. I., Vicente-Serrano, S. M., Lasanta-Martínez, T., and Beguería, S.: Mediterranean water resources in a global change scenario, 105, 121–139, https://doi.org/10.1016/J.EARSCIREV.2011.01.006, 2011.

Gilleland, E. and Katz, R. W.: extRemes 2.0: An Extreme Value Analysis Package in R, 72, 1–39, https://doi.org/10.18637/JSS.V072.I08, 2016.

Gnedenko, B.: Sur La Distribution Limite Du Terme Maximum D'Une Serie Aleatoire, 44, 423, https://doi.org/10.2307/1968974, 1943.

Goda, Y.: Inherent Negative Bias of Quantile Estimates of Annual Maximum Data Due to Sample Size Effect: A Numerical Simulation Study, 53, 397–429, https://doi.org/10.1142/S0578563411002409, 2018.

Goulden, C.: Methods of statistical analysis., 1939.

Hao, Z., Singh, V. P., and Hao, F.: Compound Extremes in Hydroclimatology: A Review, 10, 718, https://doi.org/10.3390/W10060718, 2018.

Hersbach, H., Bell, B., Berrisford, P., Hirahara, S., Horányi, A., Muñoz-Sabater, J., Nicolas, J., Peubey, C., Radu, R., Schepers, D., Simmons, A., Soci, C., Abdalla, S., Abellan, X., Balsamo, G., Bechtold, P., Biavati, G., Bidlot, J., Bonavita, M., de Chiara, G., Dahlgren, P., Dee, D., Diamantakis, M., Dragani, R., Flemming, J., Forbes, R., Fuentes, M., Geer, A., Haimberger, L., Healy, S., Hogan, R. J., Hólm, E., Janisková, M., Keeley, S., Laloyaux, P., Lopez, P., Lupu, C., Radnoti, G., de Rosnay, P., Rozum, I., Vamborg, F., Villaume, S., and Thépaut, J. N.: The ERA5 global reanalysis, 146, 1999–2049, https://doi.org/10.1002/QJ.3803, 2020.

Hochman, A., Marra, F., Messori, G., Pinto, J., Raveh-Rubin, S., Yosef, Y., and Zittis, G.: ESD Reviews: Extreme Weather and Societal Impacts in the Eastern Mediterranean, 1–53, https://doi.org/10.5194/ESD-2021-55, 2021.

Houston, T. G., Changnon, S. A., Ae, T. G. H., and Changnon, S. A.: Freezing rain events: a major weather hazard in the conterminous US, 40, 485–494, https://doi.org/10.1007/S11069-006-9006-0, 2006.

James Pickands: Statistical Inference Using Extreme Order Statistics, 3, 119–131, https://doi.org/10.1214/AOS/1176343003, 1975.

Konisky, D. M., Hughes, L., and Kaylor, C. H.: Extreme weather events and climate change concern, 134, 533–547, https://doi.org/10.1007/S10584-015-1555-3/FIGURES/3, 2016.

Kundzewicz, Z. W., Radziejewski, M., and Pińskwar, I.: Precipitation extremes in the changing climate of Europe, 31, 51–58, https://doi.org/10.3354/CR031051, 2006.

Lazoglou, G. and Anagnostopoulou, C.: Joint distribution of temperature and precipitation in the Mediterranean, using the Copula method, 135, 1399–1411, https://doi.org/10.1007/S00704-018-2447-Z/FIGURES/5, 2019.

Lemus-Canovas, M.: Changes in compound monthly precipitation and temperature extremes and their relationship with teleconnection patterns in the Mediterranean, Journal of Hydrology, 608, 127580, https://doi.org/10.1016/J.JHYDROL.2022.127580, 2022.

Leonard, M., Westra, S., Phatak, A., Lambert, M., van den Hurk, B., Mcinnes, K., Risbey, J., Schuster, S., Jakob, D., and Stafford-Smith, M.: A compound event framework for understanding extreme impacts, 5, 113–128, https://doi.org/10.1002/WCC.252, 2014.

Lhotka, O. and Kyselý, J.: Precipitation–temperature relationships over Europe in CORDEX regional climate models, International Journal of Climatology, https://doi.org/10.1002/JOC.7508, 2021.

Llasat, M. C., Turco, M., Quintana-Seguí, P., and Llasat-Botija, M.: The snow storm of 8 March 2010 in Catalonia (Spain): a paradigmatic wet-snow event with a high societal impact, 14, 427–441, https://doi.org/10.5194/NHESS-14-427-2014, 2014.

Markantonis, I., Vlachogiannis, D., Sfetsos, T., Kioutsioukis, I., and Politi, N.: An Investigation of cold-wet Compound Events in Greece, https://doi.org/10.5194/EMS2021-188, 2021.

Moalafhi, D. B., Evans, J. P., and Sharma, A.: Evaluating global reanalysis datasets for provision of boundary conditions in regional climate modelling, 47, 2727–2745, https://doi.org/10.1007/S00382-016-2994-X/TABLES/9, 2016.

Moberg, A., Jones, P. D., Lister, D., Walther, A., Brunet, M., Jacobeit, J., Alexander, L. v., Della-Marta, P. M., Luterbacher, J., Yiou, P., Chen, D., Tank, A. M. G. K., Saladié, O., Sigró, J., Aguilar, E.,

Alexandersson, H., Almarza, C., Auer, I., Barriendos, M., Begert, M., Bergström, H., Böhm, R., Butler, C. J., Caesar, J., Drebs, A., Founda, D., Gerstengarbe, F. W., Micela, G., Maugeri, M., Österle, H., Pandzic, K., Petrakis, M., Srnec, L., Tolasz, R., Tuomenvirta, H., Werner, P. C., Linderholm, H., Philipp, A., Wanner, H., and Xoplaki, E.: Indices for daily temperature and precipitation extremes in Europe analyzed for the period 1901–2000, 111, 22106, https://doi.org/10.1029/2006JD007103, 2006.

Nelsen, R.: An introduction to copulas, 2007.

Pandey, P. K., Das, L., Jhajharia, D., and Pandey, V.: Modelling of interdependence between rainfall and temperature using copula, 4, 867–879, https://doi.org/10.1007/S40808-018-0454-9, 2018.

Pestereva, N. M., Popova, N. Yu., and Shagarov, L. M.: Modern Climate Change and Mountain Skiing Tourism: the Alps and the Caucasus, 1602–1617, 2012.

Politi, N., Nastos, P. T., Sfetsos, A., Vlachogiannis, D., and Dalezios, N. R.: Evaluation of the AWR-WRF model configuration at high resolution over the domain of Greece, 208, 229–245, https://doi.org/10.1016/J.ATMOSRES.2017.10.019, 2018.

Politi, N., Sfetsos, A., Vlachogiannis, D., Nastos, P. T., and Karozis, S.: A Sensitivity Study of High-Resolution Climate Simulations for Greece, 8, 44, https://doi.org/10.3390/CLI8030044, 2020.

Politi, N., Vlachogiannis, D., Sfetsos, A., and Nastos, P. T.: High-resolution dynamical downscaling of ERA-Interim temperature and precipitation using WRF model for Greece, 57, 799–825, https://doi.org/10.1007/S00382-021-05741-9/FIGURES/17, 2021.

Politi, N., Vlachogiannis, D., Sfetsos, A., Nastos, P.T., High resolution projections for extreme temperatures and precipitation over Greece, under review, https://doi.org/10.21203/rs.3.rs-1263740/v1, 2022

Pongrácz, R., Bartholy, J., Gelybó, G., and Szabó, P.: Detected and expected trends of extreme climate indices for the carpathian basin, 15–28, https://doi.org/10.1007/978-1-4020-8876-6_2, 2009.

Raziei, T., Daryabari, J., Bordi, I., Modarres, R., and Pereira, L. S.: Spatial patterns and temporal trends of daily precipitation indices in Iran, 124, 239–253, https://doi.org/10.1007/S10584-014-1096-1/TABLES/1, 2014.

Rockel, B., Will, A., and Hense, A.: The regional climate model COSMO-CLM (CCLM), 17, 347–348, https://doi.org/10.1127/0941-2948/2008/0309, 2008.

Sadegh, M., Moftakhari, H., Gupta, H. v., Ragno, E., Mazdiyasni, O., Sanders, B., Matthew, R., and AghaKouchak, A.: Multihazard Scenarios for Analysis of Compound Extreme Events, 45, 5470–5480, https://doi.org/10.1029/2018GL077317, 2018.

Samuelsson, P., Jones, C. G., Willén, U., Ullerstig, A., Gollvik, S., Hansson, U., Jansson, C., Kjellström, E., Nikulin, G., and Wyser, K.: The Rossby Centre Regional Climate model RCA3: model description and performance, 63, 4–23, https://doi.org/10.1111/J.1600-0870.2010.00478.X, 2016.

Schepsmeier, U., Stoeber, J., Christian, E., and Maintainer, B.: Package “VineCopula” Type Package Title Statistical inference of vine copulas, 2013.

Schwarz, G.: Estimating the Dimension of a Model, https://doi.org/10.1214/aos/1176344136, 6, 461–464, https://doi.org/10.1214/AOS/1176344136, 1978.

Singh, H., Najafi, M. R., and Cannon, A. J.: Characterizing non-stationary compound extreme events in a changing climate based on large-ensemble climate simulations, 56, 1389–1405, https://doi.org/10.1007/S00382-020-05538-2/FIGURES/6, 2021.

Sklar and M.: Fonctions de repartition a n dimensions et leurs marges, 8, 229–231, 1959.

Spiridonov, V., Somot, S., and Déqué, M.: ALADIN-Climate: from the origins to present date, n.d.

Tavakol, A., Rahmani, V., and Harrington, J.: Probability of compound climate extremes in a changing climate: A copula-based study of hot, dry, and windy events in the central United States, 15, 104058, https://doi.org/10.1088/1748-9326/ABB1EF, 2020.

Tošić, I. and Unkašević, M.: Extreme daily precipitation in Belgrade and their links with the prevailing directions of the air trajectories, 111, 97–107, https://doi.org/10.1007/S00704-012-0647-5/FIGURES/9, 2013.

Tringa E and Kostopoulou E: An observational study of the relationships between extreme temperature and precipitation and the surface atmospheric circulation in Greece, n.d.

Trujillo, E., Molotch, N. P., Goulden, M. L., Kelly, A. E., and Bales, R. C.: Elevation-dependent influence of snow accumulation on forest greening, 5, 705–709, https://doi.org/10.1038/ngeo1571, 2012.

Vajda, A., Tuomenvirta, H., Juga, I., Nurmi, P., Jokinen, P., and Rauhala, J.: Severe weather affecting European transport systems: The identification, classification and frequencies of events, 72, 169–188, https://doi.org/10.1007/S11069-013-0895-4/TABLES/3, 2014.

van Meijgaard, E., van Ulft, L. H., van de Berg, W. J., Bosveld, F. C., van den Hurk, B. J. J. M., Lenderink, G., and Siebesma, A. P.: The KNMI regional atmospheric climate model RACMO version 2.1, 2008.

Vogel, J., Paton, E., and Aich, V.: Seasonal ecosystem vulnerability to climatic anomalies in the Mediterranean, 18, 5903–5927, https://doi.org/10.5194/BG-18-5903-2021, 2021.

Voudouri, A. and Kotta, D.: Factors Determined Snow Accumulation Over the Greater Athens Area During the Latest Snowfall Events, 355–361, https://doi.org/10.1007/978-3-642-29172-2_50, 2013.

Zanocco, C., Boudet, H., Nilson, R., Satein, H., Whitley, H., and Flora, J.: Place, proximity, and perceived harm: extreme weather events and views about climate change, 149, 349–365, https://doi.org/10.1007/S10584-018-2251-X/TABLES/2, 2018.

Zhang, W., Luo, M., Gao, S., Chen, W., Hari, V., and Khouakhi, A.: Compound Hydrometeorological Extremes: Drivers, Mechanisms and Methods, 9, 941, https://doi.org/10.3389/FEART.2021.673495/BIBTEX, 2021.

Zscheischler, J. and Seneviratne, S. I.: Dependence of drivers affects risks associated with compound events, 3, https://doi.org/10.1126/SCIADV.1700263/SUPPL_FILE/1700263_SM.PDF, 2017.

Zscheischler, J., Orth, R., and Seneviratne, S. I.: Bivariate return periods of temperature and precipitation explain a large fraction of European crop yields, 14, 3309–3320, https://doi.org/10.5194/BG-14-3309-2017, 2017.

Zscheischler, J., Westra, S., van den Hurk, B. J. J. M., Seneviratne, S. I., Ward, P. J., Pitman, A., AghaKouchak, A., Bresch, D. N., Leonard, M., Wahl, T., and Zhang, X.: Future climate risk from compound events, 8, 469–477, https://doi.org/10.1038/s41558-018-0156-3, 2018.

Zhou, S., Zhang, Y., Williams, A. P., and Gentine, P.: Projected increases in intensity, frequency, and terrestrial carbon costs of compound drought and aridity events, Science Advances, 5, https://doi.org/10.1126/SCIADV.AAU5740/SUPPL_FILE/AAU5740_SM.PDF, 2019.

Code and data availability

Code and results data available upon request.

Author contributions

IM has worked on conceptualization, methodology, validation, visualization, investigation, writing review and editing. AS, DV and IK contributed on conceptualization, review and supervision. All authors have read and agreed to the published version of the manuscript.

Competing interests

The authors declare that they have no conflict of interest.

Appendix A

NUMBER	LOCATION	ID	LATITUDE	LONGITUDE	ELEVATION (m)
1	Alexandroupoli	16627	40.85	25.917	4
2	Elliniko	16716	37.8877	23.7333	10
3	Ioannina	16642	39.7	20.817	483
4	Irakleio	16754	35.339	25.174	39
5	Kalamata	16726	37.067	22.017	6
6	Kastoria	16614	40.45	21.28	660.95
7	Kerkira	16641	39.603	19.912	1
8	Kithira	16743	36.2833	23.0167	167
9	Larisa	16648	39.65	22.417	73
10	Limnos	16650	39.9167	25.2333	4
11	Methoni	16734	36.8333	21.7	34
12	Milos	16738	36.7167	24.45	183
13	Mitilini	16667	39.059	26.596	4
14	Naxos	16732	37.1	25.383	9
15	Rhodes	16749	36.42896	28.21661	95
16	Samos	16723	37.79368	26.68199	10
17	Skyros	16684	38.9676	24.4872	12
18	Souda	16746	35.4833	24.1167	151
19	Thessaloniki	16622	40.517	22.967	2
20	Tripoli	16710	37.527	22.401	651
21	Zakinthos	16719	37.751	20.887	5

Table A1: HNMS stations information.